Supporting Information

Gao and Stock 10.1073/pnas.1214587110

SI Materials and Methods

Strains and Plasmids. The strains and plasmids used in this study are listed in Table S2. λ red recombination (1) was used to make chromosomal gene disruption or alteration in strain BW25113 or derivatives of BW25113. To disrupt the *phoBR* operon, the *phoBR* gene was replaced by the kanamycin resistance Km^r cassette amplified from pKD13 using primers RG29 (5′-GATCGCAACCTATTTATTACAACAGGGCAAATCATGGCGAGTGTAGGCTGGAGCTGCTTC-3′) and RG83 (5′-GGCGGATTAATCGCTGTTTTTGGCAATTAAACGTTCCGGGATTCCGGGGATCCGTCGACC-3′). The Km^r cassette was subsequently removed by FRT recombination using pCP20 to give RU1621.

We used the same λ red recombination technique to replace the PHO box (TTTTCATAAATCTGTCATA) in the *phoBR* promoter with a sequence element (CATTGACATAAAGATA) carrying the −35 consensus sequence (TTGACA) and lacking the PhoB recognition features (2). In short, primers RG147 (5′-CTGCGCCACGGAAATCAATAACCTGAAGATATGTGCGACGTGTAGGCTGGAGCTGCTTCG-3′) and RG148 (5′-ATAGGTTGCGATCATTAATGCGACGTCATTATGCGTCAGATTTATCTTTATGTCAATGATTCCGGGGATCCGTCGACC-3′) were used to amplify the Km^r cassette for λ red recombination. After elimination of the Km^r cassette, the resulting RU1617 (KON) strain has the desired −35 sequence element (underlined) upstream of the −10 region of the *phoB* promoter and additional scar sequences left from FRT recombination (1). RU1616 (LAC) and RU1618 (TRC) were created following a similar strategy to replace the autoregulated *phoB* promoter with a constitutive *lac* or *trc* promoter. Primers used included RG147, RG149 (5′-TCACTGCCCGCTTTCCAGATTCCGGGGATCCGTCGAC-3′), RG150 (5′-GTCGACGGATCCCCGGAATCTGGAAAGCGGGCAGTGA-3′), and number 175 (5′-GCCGAAGCTTCGAAATACGGCGCATTACCGC-3′). The promoter and *phoB* sequences of these strains were all confirmed by sequencing.

The promoterless *phoBR* operon was also amplified from BW25113 genomic DNA using primers number 174 (5′-GGCCGGCATATGGCGAGACGTATTCTGGTC-3′) and RG75 (5′-GCAAAGCTTTTAATCGCTGTTTTTGGCAATT-3′). The resulting product was cloned between NdeI and HindIII sites of pET21b to give pRG225, and the XbaI/NotI fragment containing *phoBR* was then moved from pRG225 to pRG2 behind the *lac* promoter to create pRG226. Recombinant PCR was used to introduce the F20D mutation to *phoB* with primers RG140 (5′-GGAATGGTGCATGCCTGGCGCCCAATACGCAAACC-3′), RG185 (5′-CCATTTTGTTCGAGCACGTCGCAGACCATTTCG-3′), RG184 (5′-CGAAATGGTCTGCGACGTGCTCGAACAAAATGG-3′), and number 127 (5′-GCCGAAGCTTAAAGCGGGTTGAAAAACGATATC-3′). The PCR fragment was digested with EcoRI/BsrGI and cloned into pRG226 to give pRG298. Similarly the fragment containing $phoB^{D53A}$ was excised from pJZG137 and cloned between EcoRI and BsrGI sites to create pRG305. The expression vector pJZG247 producing the cytoplasmic domain of PhoR ($PhoR^{cyt}$) was cloned by PCR using primers RG74 (5′-GAGCCCATATGCTGCGAAATAAAAAACGCCGC-3′) and RG75, followed by ligation into NdeI/HindIII-digested pET21b.

Phosphate Starvation. Bacteria were grown at 37 °C in 3-(*N*-morpholino)propanesulfonic acid (Mops) minimal medium (3) supplemented with 0.4% (wt/vol) glucose, amino acid mix (0.04 mg/mL for each amino acid), and indicated concentrations of phosphates (KH_2PO_4). To assay bacterial responses to phosphate concentrations, cells from overnight LB cultures were inoculated into Mops minimal media containing 2 mM KH_2PO_4 and grown to an OD_{600} between 0.3 and 0.7. Cells harvested from these fresh cultures were washed once and inoculated into Mops minimal media containing either 2 mM (Pi-rich) or 50 μM (Pi-limited) phosphates with a starting OD_{600} at 0.04 followed by 3 h growth. Bacteria cells equivalent to 0.3 OD_{600}·mL were then pelleted and assayed for protein expression, in vivo phosphorylation, and alkaline phosphatase (AP) activity. AP activities were measured as described before (4, 5) in the presence of ∼7 mM substrate, *p*-nitrophenylphosphate. The rate of absorbance change at 420 nm was multiplied by 10,000 to represent the AP activities. For time-course analyses of phosphate starvation responses, cells were grown as described above with a starting OD_{600} at 0.04 in Mops minimal media containing 50 μM phosphates. Aliquots were removed at indicated times, and bacteria pellets were stored at −80 °C for later Western and AP assays.

Protein Purification. PhoB and $PhoB^{F20D}$ proteins were purified as described before (5). $PhoR^{cyt}$ (84-431) was expressed in Rosetta (DE3) (Novagen) carrying pJZG247 with the induction of 0.5 mM IPTG for 2–3 h. Cells were lysed by sonication in 50 mM Tris·HCl, 0.1 M NaCl, and 2 mM β-mercaptoethanol (β-ME) at pH 8.0. After clarification, all native proteins were precipitated by addition of ammonium sulfate to 65% (wt/vol). The protein pellets were resuspended into a dialysis buffer of 25 mM Tris·HCl (pH 8.0), 2 mM β-ME, and dialyzed overnight. Proteins were loaded onto tandem 5-mL Heparin HiTrap columns (GE Healthcare) and eluted with a gradient of 20 mM Tris (pH 8.0), 2 mM β-ME, and 2 M NaCl. The purest eluant fractions were pooled together, concentrated, and loaded onto the Superdex 75 26/60 column preequilibrated in 25 mM Tris·HCl (pH 8.0), 0.1 M NaCl, and 2 mM β-ME. The concentrations of all proteins were calculated from their absorbance at 280 nm using extinction coefficients computed from their protein sequences.

In Vitro Phosphatase and Phosphotransfer Assays. All in vitro biochemical assays were performed at room temperature. To compare the dephosphorylation rates of $PhoB^{WT}$ and $PhoB^{F20D}$, PhoB proteins were phosphorylated by 20 mM phosphoramidate for ∼45 min in the reaction buffer (50 mM Tris·HCl, 100 mM NaCl, and 5 mM $MgCl_2$, pH 7.4), and the small-molecule phosphodonors were subsequently removed by desalting with Bio-Gel P-6 spin microcolumns (Bio-Rad). Absorbance at 280 nm was quickly monitored by Nanodrop to calculate the concentration of phosphorylated PhoB proteins. Indicated concentrations of phosphorylated PhoB proteins were mixed with $PhoR^{cyt}$ with a final PhoR concentration at 0.5 μM in the reaction buffer plus 3 mM ADP to initiate dephosphorylation. Aliquots were removed at indicated time intervals (0–45 min) and added into 4× SDS loading buffer followed by rapid freezing in ethanol dry ice bath. Samples were subjected to Phos-tag gel analyses with PhoB∼P standards running along. Protein phosphorylation was assessed by Coomassie blue staining and quantified by ImageJ. Each gel lane was plotted as a line graph of signal intensities versus running positions, and the areas of intensity peaks corresponding to individual bands were measured after the selection of baselines. Phosphorylation percentages were calculated from PhoB∼P standard curves and used to derive the concentrations of PhoB∼P.

For the autophosphatase activities of PhoB proteins, phosphorylated PhoB proteins were prepared and desalted similarly as above. The automatic loss of phosphorylation was monitored in

the identical reaction buffer as above except for the absence of $PhoR^{cyt}$ protein. Longer time intervals (0–5 h) were used due to the slower rate of autodephosphorylation. Phosphorylation percentages from Phos-tag gel analyses were fitted with a single exponential decay to give the rate of autodephosphorylation (Fig. S7).

For phosphotransfer assays, $PhoR^{cyt}$ was first phosphorylated by 3 mM ATP in the reaction buffer for over an hour. Excess ATP was removed by desalting before the phosphotransfer experiments with 2 μM PhoB. Due to the nucleotide interference of absorbance at 280 nm, phosphorylated PhoR concentration could not be accurately determined but equal amounts of PhoR proteins were used for phosphotransfer to $PhoB^{WT}$ and $PhoB^{F20D}$. The PhoR concentration was later estimated to be ~3 μM based on Coomassie blue staining with standards. Because PhoB~P ran extremely close to PhoR and PhoR~P bands, quantification was only focused on the remaining unphosphorylated PhoB protein bands instead of PhoB~P fractions. Identification of different PhoB protein bands was confirmed by Western blot analyses.

Modeling and Data Fitting. The kinetic model shown in Fig. 3*B* was the same as the previous model of the central phosphorylation cycle introduced by the Goulian Laboratory (6, 7). As described previously (6), when the total concentration of response regulator (RR) is much greater than that of histidine sensor kinase (HSK), the steady-state solution can be described by the following equation:

$$[\mathrm{RR}\sim\mathrm{P}] \approx \frac{1}{2}\left(C_t + C_p + [\mathrm{RR}]_{\mathrm{total}}\right) - \frac{1}{2}\sqrt{\left(C_t + C_p + [\mathrm{RR}]_{\mathrm{total}}\right)^2 - 4C_p[\mathrm{RR}]_{\mathrm{total}}}.$$

The concentration of phosphorylated RR is a simple function of the total concentration of RR. Dividing both sides of the equation with the total concentration of RR gives the relationship between the phosphorylation fraction and the total concentration of RR. This was used for the nonlinear curve fit of the experimental data to derive the values of C_p and C_t.

The success of the modeling requires that a few assumptions be satisfied by the specific TCS phosphorylation reactions. One major assumption is that RRs are in great excess to HSKs, so that a simple function can be used to describe the relationship between RR~P and total RR amount. The PhoR/PhoB system displayed a high ratio of RR to HSK, which is also observed for the PhoQ/PhoP and EnvZ/OmpR systems where the model agreed well with experiments (6–8). Second, the rate of RR autodephosphorylation is assumed to be negligible compared with the rate of phosphatase-catalyzed RR dephosphorylation. Dephosphorylation of PhoB by $PhoR^{cyt}$ in vitro indicated a much larger phosphatase rate constant k_p than the autodephosphorylation rate constant k_γ. This may well hold true for full-length proteins in vivo considering that phosphatase activity is usually attenuated in truncated HSK proteins due to the lack of regulation from sensory domains. All these contribute to the agreement of the model with experimental PhoB phosphorylation data.

For the inactive dimer model presented in Fig. S6, the formation of the inactive dimer is assumed to be in a fast equilibrium defined by the dissociation constant K_d. Thus, the concentration of the inactive dimer is expressed as the following:

$$[\mathrm{Dimer}_{\mathrm{inactive}}] = \frac{[\mathrm{RR}]^2}{K_d}.$$

Given the high ratio of RR over HSK, the concentration of RR–HSK complex is negligible and we take $[\mathrm{RR}]_{\mathrm{total}} \approx [\mathrm{RR}\sim\mathrm{P}] + [\mathrm{RR}] + 2[\mathrm{Dimer}_{\mathrm{inactive}}]$. The steady solutions were numerically computed with MATLAB for different values of K_d and plotted in Fig. S6.

To consider the effect of PhoB autodephosphorylation on in vitro phosphatase assays, a kinetic model was explored with the Simbiology tool of the MATLAB package. It has been reported that binding of nucleotides, such as ADP, ATP, or ATP analogs, exerts complicated effects on HSK phosphatase activities (9, 10). The ADP concentration used in dephosphorylation experiments (3 mM) was higher than the physiological concentration, but the great excess of ADP to $PhoR^{cyt}$ ensures saturated binding. The complicacy caused by different amount of nucleotide-bound or apo- forms of $PhoR^{cyt}$ can be minimized. A simple model considering the reversible binding of PhoB~P with PhoR and the dephosphorylation reaction were as follows:

$$\mathrm{PhoB}\sim\mathrm{P} + \mathrm{PhoR} \Leftrightarrow (\mathrm{PhoR}\cdot\mathrm{PhoB}\sim\mathrm{P}) \rightarrow \mathrm{PhoB} + \mathrm{PhoR} + \mathrm{Pi}.$$

The reverse rate constant of the binding, k_{-1}, the Michaelis–Menten kinetic parameters K_m and k_p were sufficient to describe the kinetics of the PhoR-mediated dephosphorylation. With experimentally determined K_m, k_p, and k_γ values, the PhoB~P concentrations were simulated with different k_{-1} values using MATLAB and no significant difference was observed given a similar K_m. Different K_m and k_p values as described in Fig. 5 were used for simulations to compare with experimental dephosphorylation data of $PhoB^{F20D}$.

1. Datsenko KA, Wanner BL (2000) One-step inactivation of chromosomal genes in *Escherichia coli* K-12 using PCR products. *Proc Natl Acad Sci USA* 97(12):6640–6645.
2. Blanco AG, Sola M, Gomis-Rüth FX, Coll M (2002) Tandem DNA recognition by PhoB, a two-component signal transduction transcriptional activator. *Structure* 10(5): 701–713.
3. Neidhardt FC, Bloch PL, Smith DF (1974) Culture medium for enterobacteria. *J Bacteriol* 119(3):736–747.
4. Gao R, Tao Y, Stock AM (2008) System-level mapping of *Escherichia coli* response regulator dimerization with FRET hybrids. *Mol Microbiol* 69(6):1358–1372.
5. Mack TR, Gao R, Stock AM (2009) Probing the roles of the two different dimers mediated by the receiver domain of the response regulator PhoB. *J Mol Biol* 389(2): 349–364.
6. Miyashiro T, Goulian M (2008) High stimulus unmasks positive feedback in an autoregulated bacterial signaling circuit. *Proc Natl Acad Sci USA* 105(45): 17457–17462.
7. Cai SJ, Inouye M (2002) EnvZ-OmpR interaction and osmoregulation in *Escherichia coli*. *J Biol Chem* 277(27):24155–24161.
8. Batchelor E, Goulian M (2003) Robustness and the cycle of phosphorylation and dephosphorylation in a two-component regulatory system. *Proc Natl Acad Sci USA* 100(2):691–696.
9. Yeo WS, et al. (2012) Intrinsic negative feedback governs activation surge in two-component regulatory systems. *Mol Cell* 45(3):409–421.
10. Huynh TN, Stewart V (2011) Negative control in two-component signal transduction by transmitter phosphatase activity. *Mol Microbiol* 82(2):275–286.

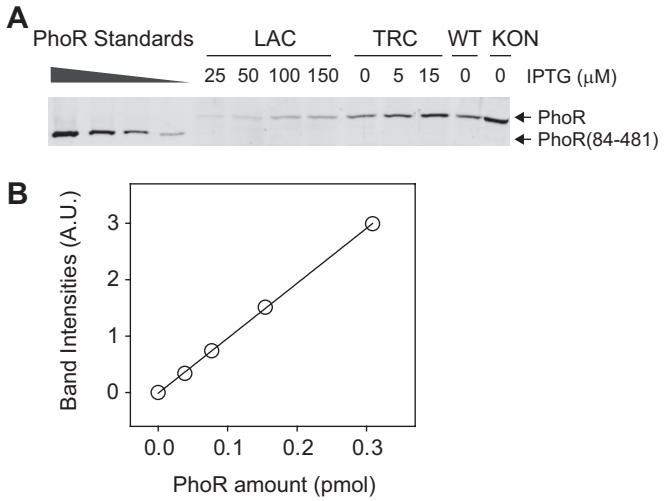

Fig. S1. Quantification of PhoR expression. (*A*) Quantitative Western analyses of PhoR expression. Pure $PhoR^{cyt}$ proteins were used as standards; thus, the molecular weight appeared smaller than that of the full-length PhoR protein. (*B*) Quantification of PhoR standards. Band intensities follow a linear relationship with actual PhoR amount, and this fitted standard curve was used to calculate the PhoR concentration in the samples.

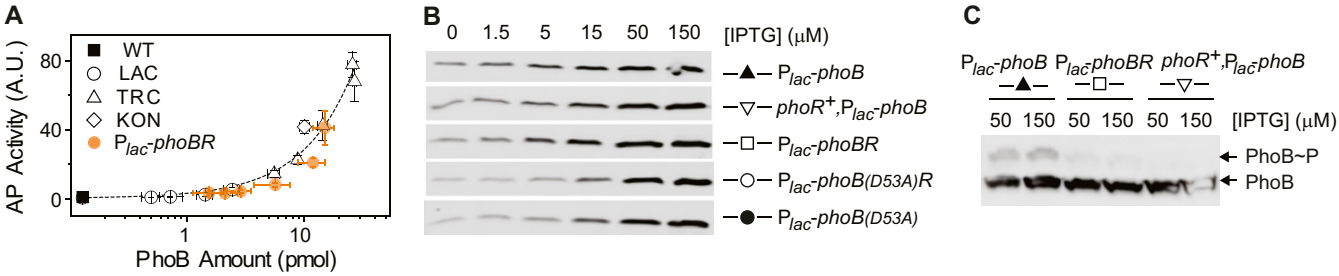

Fig. S2. Effect of PhoB/PhoR levels on basal activities under Pi-replete conditions. (*A*) Increasing basal AP activities with higher protein expression. Similar dependence of AP activities on protein levels were observed for strains with PhoB/PhoR expressing from the chromosome (WT, LAC, TRC, and KON) or from the plasmid (RU1621/pRG226; orange circles). (*B*) Similar protein levels for strains expressing PhoB from plasmids. Strains used are as follows: from top to bottom, RU1621/pTRM11, RU1631/pTRM11, RU1621/pRG226, RU1621/pRG305, and RU1621/pJZG137. (*C*) Phosphorylation suppression by PhoR. Expression of PhoR either at a low level from the chromosome (open triangle) or at a high level from the plasmid (open square) suppressed the nonspecific phosphorylation observed for the strain without *phoR* (solid triangle).

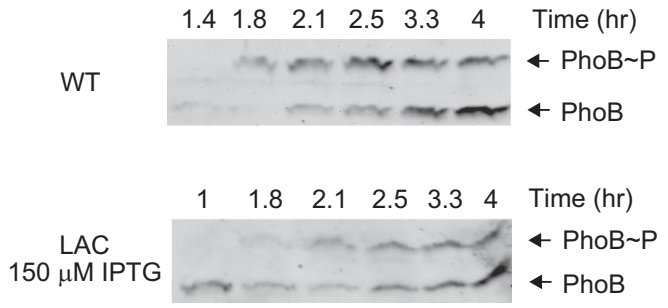

Fig. S3. Time course of PhoB Phosphorylation. As indicated in Table S1, expression levels of PhoB are similar for the constitutive LAC strain induced by 150 μM IPTG (*Lower*) and the autoregulated wild type BW25113 strain (*Upper*) under Pi-limited conditions. Both strains were grown in Mops medium containing 50 μM Pi, and the kinetics of phosphate starvation response were followed as described in *Materials and Methods*. Both reached steady state of phosphorylation after 2.5 h.

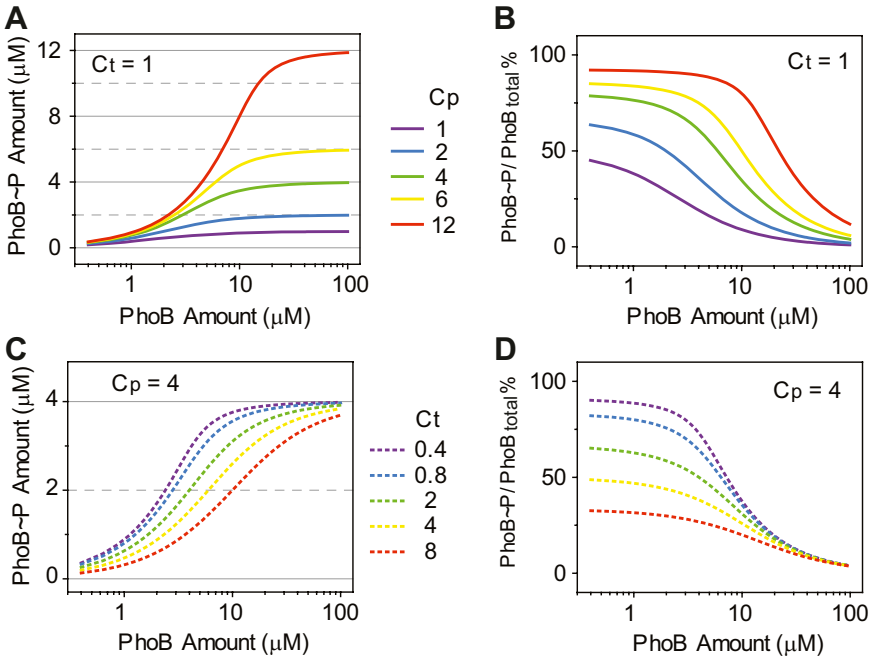

Fig. S4. Effect of C_p (*A* and *B*) and C_t (*C* and *D*) on modeled phosphorylation levels of PhoB. Absolute phosphorylation levels (*A* and *C*) and phosphorylation percentages (*B* and *D*) are shown, respectively. Phosphorylation saturates at the level of C_p. Given a similar C_p, higher C_t requires higher protein level to reach saturation. Phosphorylation percentages are dependent on both C_p and C_t.

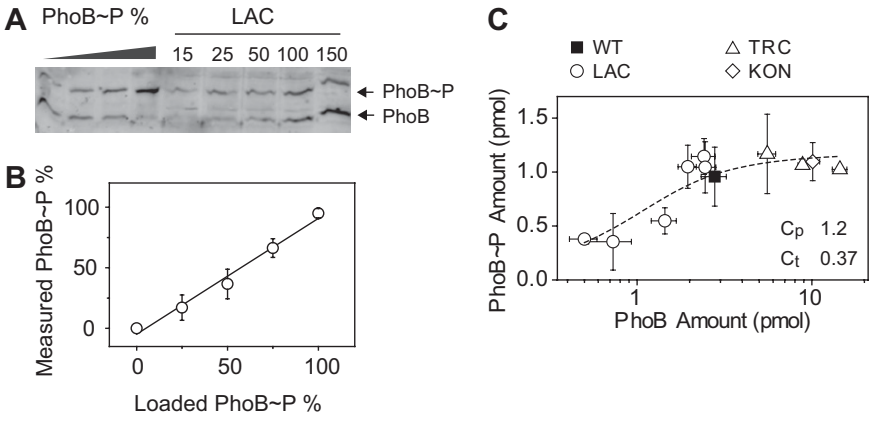

Fig. S5. Quantification of in vivo phosphorylation. (*A*) Example of Phos-tag analyses with PhoB~P standards. Phosphorylation levels were analyzed for the indicated strain under Pi-limited conditions. Known fractions of PhoB~P proteins were loaded as standards. (*B*) Standard curve of the measured phosphorylation percentages versus the loaded phosphorylation fractions. The solid line represents the best linear fit. (*C*) Saturation of PhoB phosphorylation levels. In contrast to the data in Fig. 3*C* where both PhoB~P and unphosphorylated PhoB bands were used to calculate phosphorylation fractions, phosphorylation levels in this figure were computed using only the intensities of upper PhoB~P bands. Fitting the data (dashed line) gave a C_p at 1.2 pmol and C_t at 0.37 pmol, similar to the values fitted from the phosphorylation percentages shown in Fig. 3*C*. Error bars are SDs from at least three independent experiments.

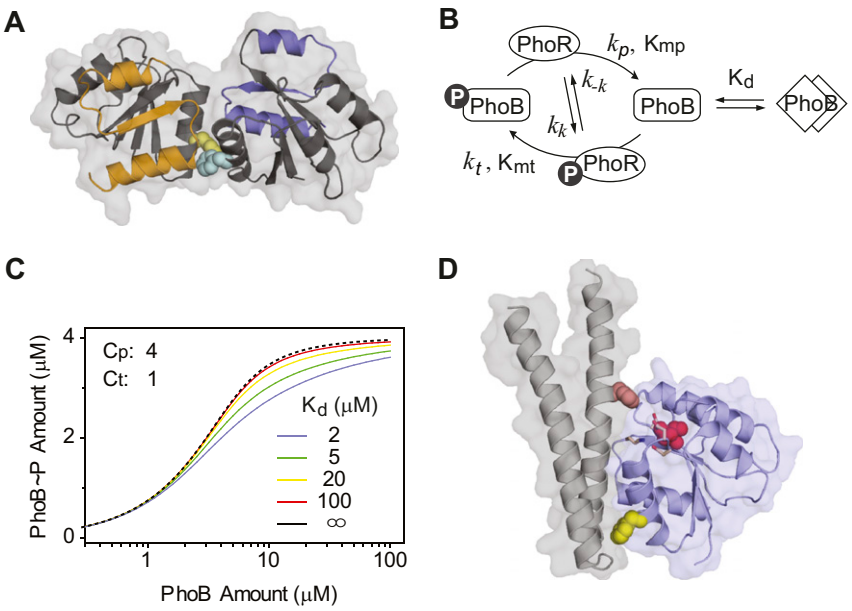

Fig. S6. Roles of the F20 residue. (*A*) Inactive dimer conformation of PhoB. The F20 residues (colored in yellow and cyan) constitute the core contacts between the two subunits. Formation of this alternative dimer is suggested to prevent the active dimer interfaces (colored in orange and violet) to contact each other (1, 2). Thus, it shifts the conformation equilibrium to inactive states that limit the PhoB activity. (*B*) Model of the inactive dimer. A fast equilibrium of inactive dimer formation was included with the phosphorylation model. (*C*) Simulated curves with different K_d values for inactive dimers. It predicts that the formation of inactive dimers will cause noticeable decrease on steady-state phosphorylation only when the K_d is at the same order of magnitude as C_p and C_t. It cannot account for the observed higher phosphorylation of PhoB^{F20D}. (*D*) Structure of the HK853–RR468 complex (Protein Data Bank ID code 3DGE). There is no structure available for the PhoR–PhoB complex, but PhoB shares a similar fold as RR468 whose interactions with HSKs have been structurally characterized (3). At the same position of F20 in PhoB, RR468 also has a Phe residue (yellow) and the residue is involved in HSK–RR interactions. It is also far from the phosphorylation site colored in red. The histidine kinase HK853 is in gray, whereas the RR468 is in light blue.

1. Mack TR, Gao R, Stock AM (2009) Probing the roles of the two different dimers mediated by the receiver domain of the response regulator PhoB. *J Mol Biol* 389(2):349–364.
2. Batchelor E, Goulian M (2003) Robustness and the cycle of phosphorylation and dephosphorylation in a two-component regulatory system. *Proc Natl Acad Sci USA* 100(2):691–696.
3. Casino P, Rubio V, Marina A (2009) Structural insight into partner specificity and phosphoryl transfer in two-component signal transduction. *Cell* 139(2):325–336.

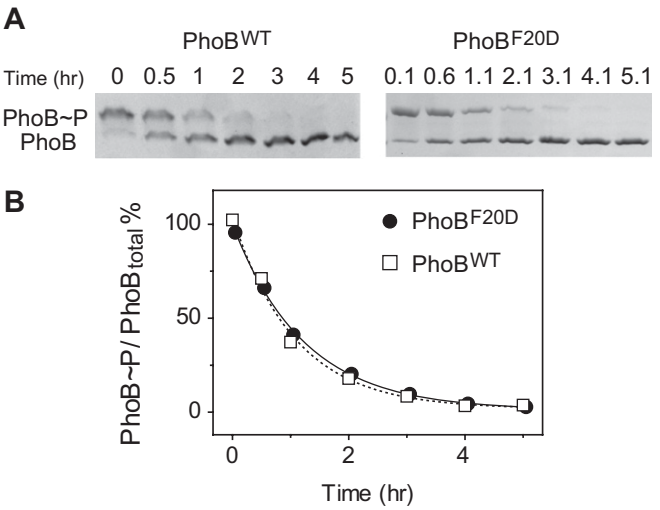

Fig. S7. (*A*) Autodephosphorylation of PhoB^{WT} (*Left*) and PhoB^{F20D} (*Right*). (*B*) Determination of the autodephosphorylation rate constants. The solid and dotted lines represent single exponential decay curves for PhoB^{WT} and PhoB^{F20D}, respectively. Only one experiment is shown. Decay constants from three independent experiments were averaged to give k_γ values: PhoB^{WT}, 2.6 ± 0.27 s^{-1}; PhoB^{F20D}, 2.4 ± 0.23 s^{-1}.

Table S1. Quantification of PhoB and PhoR levels

Strains/conditions	PhoB amount, pmol	PhoR amount, pmol
WT (BW25113)		
Pi-replete	0.13*	ND†
Pi-limited	2.79 ± 0.46	0.30 ± 0.10
KON	10.1 ± 1.0	1.02 ± 0.20
LAC w/IPTG		
0 μM	0.13*	ND
15 μM	0.50 ± 0.09	ND
25 μM	0.73 ± 0.20	0.07 ± 0.01
50 μM	1.44 ± 0.24	0.11 ± 0.02
75 μM	1.95 ± 0.23	ND
100 μM	2.42 ± 0.37	0.23 ± 0.02
150 μM	2.45 ± 0.37	0.22 ± 0.06
TRC w/IPTG		
0 μM	5.56 ± 0.64	0.39 ± 0.09
5 μM	8.85 ± 0.52	0.67 ± 0.12
15 μM	14.5 ± 1.4	0.94 ± 0.07
50 μM	27.0 ± 1.0	ND
150 μM	25.9 ± 2.2	ND
pRG226 w/IPTG		
0 μM	1.55 ± 0.42	ND
1.5 μM	2.11 ± 0.59	ND
5 μM	2.87 ± 0.66	0.38 ± 0.06
15 μM	5.67 ± 1.91	ND
50 μM	11.9 ± 3.0	1.00 ± 0.24
150 μM	15.0 ± 3.1	ND

Protein levels were determined from 0.3 OD·mL of cells using Western blot with pure proteins as standards. Quantification values are shown as the mean ± SD from at least three independent experiments.
*Number is determined based on the relative ratio to Pi-limited WT samples.
†ND, not determined.

Table S2. Strains and plasmids used in this study

Strains/plasmids	Relevant characteristics	Source
Strains *E. coli*		
DH5α	General cloning strain	Invitrogen
BL21(DE3)	F^-, *ompT*, *hsdS*$_B$(r_B-, m_B-), *dcm*, *gal*, λ(DE3)	Novagen
BW25113	Wild type, *lacI* ^{q} *rrnB*$_{T14}$ Δ*lacZ*$_{WJ16}$ *hsdR514* Δ*araBA-D*$_{AH33}$ Δ*rhaBAD*$_{LD78}$	Ref. 1
BW27784	BW25113 derivative, DE(*araFGH*) Φ(Δ*araEp* P$_{cp18}$-*araE*)	Ref. 2
JWK0389-1	Δ*phoB*::*kan* in BW25113	Ref. 3
RU1631	Δ*phoB* in BW25113	This study
RU1616	LAC, Φ(Δ*phoBp* P$_{lac}$-*phoBR*) in BW25113	This study
RU1617	KON, Φ(Δ*phoBp phoBR*) replacement of phoB box with −35 sequence in BW25113	This study
RU1618	TRC, Φ(Δ*phoBp* P$_{trc}$-*phoBR*) in BW25113	This study
RU1621	Δ*phoBR* in BW27784	This study
Plasmids		
pET21b	T7 polymerase-based expression vector, Ap^r	Novagen
pTRM3	PhoB expression vector (T7), Ap^r	Ref. 4
pTRM52	PhoB^{F20D}-6xHis expression vector (T7), Ap^r	Ref. 4
pJZG137	*P$_{lac}$-phoB*^{D53A}, Ap^r	This study
pJZG247	PhoR(84-431 aa) expression vector, pET21b derivative, Ap^r	This study
pTRM11	*P$_{lac}$-phoB*, Ap^r	Ref. 4
pRG2	*lac* promoter with multicloning site, Ap^r	This study
pRG225	*phoBR* in pET21b, Ap^r	This study
pRG226	*P$_{lac}$-phoBR*, pRG2 derivative, Ap^r	This study
pRG298	*P$_{lac}$-phoB*^{F20D}*phoR*, pRG2 derivative, Ap^r	This study
pRG305	*P$_{lac}$-phoB*^{D53A}*phoR*, pRG2 derivative, Ap^r	This study

1. Datsenko KA, Wanner BL (2000) One-step inactivation of chromosomal genes in *Escherichia coli* K-12 using PCR products. *Proc Natl Acad Sci USA* 97(12):6640–6645.
2. Khlebnikov A, Datsenko KA, Skaug T, Wanner BL, Keasling JD (2001) Homogeneous expression of the P(BAD) promoter in *Escherichia coli* by constitutive expression of the low-affinity high-capacity AraE transporter. *Microbiology* 147(Pt 12):3241–3247.
3. Baba T, et al. (2006) Construction of *Escherichia coli* K-12 in-frame, single-gene knockout mutants: The Keio collection. *Mol Syst Biol* 2:2006:0008.
4. Mack TR, Gao R, Stock AM (2009) Probing the roles of the two different dimers mediated by the receiver domain of the response regulator PhoB. *J Mol Biol* 389(2):349–364.